Nuclear Materials and Energy 36 (2023) 101492

Contents lists available at ScienceDirect

Nuclear Materials and Energy

journal homepage: www.elsevier.com/locate/nme

Nanostructure formation and D retention in redeposited-like W exposed to linear plasmas

D. Dellasega [a,b,*], G. Alberti [a], E. Fortuna-Zalesna [c], W. Zielinski [c], A. Pezzoli [a], S. Möller [d], B. Unterberg [d], M. Passoni [a,b], A. Hakola [e]

[a] Department of Energy, Politecnico di Milano, Milan, Italy
[b] Istituto per la Scienza e Tecnologia dei Plasmi, CNR, Milan, Italy
[c] Faculty of Materials Science and Engineering, Warsaw University of Technology, Association EURATOM-IPPLM, Warsaw, Poland
[d] Forschungszentrum Jülich GmbH, Institut für Energie- und Klimaforschung—Plasmaphysik, Jülich, Germany
[e] VTT, P. O. Box 1000, 02044 VTT, Finland

ARTICLE INFO

Keywords:
Redeposited W
Nanostructure formation
Linear machine
D retention

ABSTRACT

Different kinds of W layers resembling the ones found after campaigns in tokamak were produced by Pulsed Laser Deposition: namely nanocrystalline, amorphous and porous W layers. Films were exposed to divertor relevant D plasma, in PSI-2; D retention as well as nanostructure formation were investigated. For nanocrystalline W films we found lamellar structures that coalesce with increasing D fluence. Instead, on amorphous W no lamellas were formed but a new random string-like shape. A higher oxygen content in the W layer results in an evolution of the shape of the nanostructures in straight parallel lines with acute angles. The presence of a porous structure morphology hinders the formation of surface nanostructures. Reviewing results from different linear devices including also bulk W, we observe that, when formed, nanostructures appear in general with a fluence threshold of 3–5 $\times 10^{25}$ D/m^2 regardless the impinging D flux. D retention shows an unusual trend increasing fluence and is enhanced by the presence of amorphous structure and open morphology. Amorphous W films exhibit higher D retention (3 orders of magnitude) compared to crystalline W. When the amorphous W is annealed, retention returns to the standard values of bulk W regardless the presence of a layered structure parallel to the substrate. Porous W, thanks to the high surface to volume ratio and the presence of void distribution along the growth direction, favors higher recycling and thus limits the D uptake during exposure. The presence of O, in the investigated coatings, seems to have little effect on D retention.

Introduction

Tungsten (W), thanks to its thermo-mechanical properties (high melting temperature, high thermal conductivity) together with low erosion yield by plasma bombardment, hydrogen isotopes permeation and inventory, is the material of choice for plasma facing components (PFCs) in fusion reactors [1]. W is used for PFCs in operating tokamaks, e.g. the full first wall of ASDEX-Upgrade (AUG) and WEST and the divertor region of JET-ILW and EAST, as well as its use in future devices (e.g. ITER and DEMO). Together with Be it is one of the most studied materials in the framework of PFC [2].

Despite its suitable properties related to a bulk microcrystalline material, in the tokamak environment the surface of W undergoes several changes, due to the interaction with the peripherical fusion plasma, that lead to modifications of W PFCs becoming damaged or eroded. The released material may contribute to the formation of dust in the reactor or accumulate as re/co-deposited layers on other PFC surfaces or inside remote areas. The properties of redeposited materials may be very different in terms of composition, morphology, crystallinity and thickness depending on the first wall material, the location in the plasma chamber and the applied parameters for the plasma discharges [3]. An example is represented by AUG (2009 – 2013) campaigns, where redeposited W layers of porous nanostructured “foam like” W, 200–1500 nm thick, were found at the outer strike-point divertor tile. On the other side, compact redeposited layers were found in the outer target (tile1) of AUG [4].

In addition, because of the intrinsic pulsed regime of the tokamak machine, often redeposited material exhibits a multi-layered structure

* Corresponding author.
E-mail address: david.dellasega@polimi.it (D. Dellasega).

https://doi.org/10.1016/j.nme.2023.101492
Received 22 June 2023; Received in revised form 10 August 2023; Accepted 24 August 2023
Available online 25 August 2023

Table 1
Plasma exposure conditions.

Exposure	Exp. samples	Flux (D/m^2·s)	T_e (eV)	T_{sub} (°C)	Energy of ions (eV)
Exp.1	a-W a-W ann. p-W	1.30 x 10^{22}	8	210	40
Exp. 2	a-W(O)	6.90 x 10^{21}	10	298	50

Table 2
exposure time and fluence.

Exposure	time (min)	Fluence (D/m^2)
Exp. 1	5	3.90 x 10^{24}
	30	2.34 x 10^{25}
	60	4.68 x 10^{25}
	130	1.01 x 10^{26}
	260	2.03 x 10^{26}
Exp. 2	240	9.94 x 10^{25}

with a periodicity of tens to hundreds of nm. The composition of such films is usually W with inclusions of impurities and fuel that co-deposit with it. Typical co-deposited species are nitrogen (N), argon (Ar) and neon (Ne) coming from seeding, oxygen (O) as a residual of vents, boron (B) used for wall conditioning, and other wall materials, such as carbon (C), beryllium (Be) and steel metal components [3 4 5]. Similar features of the redeposited coatings were found during the examination of the ILW of JET after the 2013–2014 campaign and after C3 and C4 campaigns in WEST. Stratified layered morphology, both porous and compact, composed of Be, O, W and Ni were found in JET [6,7]. Stratified deposits rich in B and with metallic compounds were also found in WEST [8,9]. Such redeposited material is likely to modify the plasma wall interaction with respect to the pristine polycrystalline W (PCW), affecting both fuel retention and erosion properties as well as the formation of nanostructures.

It is widely known that the interaction of He plasmas with PCW over a certain temperature threshold and flux results in the formation of the fiber form "fuzzy" nanostructure that forms a micrometric thick layer on the PCW surface [10,11]. This peculiar structure attracted the attention of many scientists due to the possible implications in D retention and dust formation. In addition to fuzzy W, planar surface nanostructures (SNs) have been found after the interaction of W with He fluxes under the fuzzy formation threshold [12]. D fluxes on W result in the formation of a structured surface as well. Triangular, spongy, and lamellar structures have been found after interaction with low energy (38 eV) D plasma with a flux of 10^{24} m^{-2} s^{-1}. The appearance of the different shapes is related to the crystalline orientation of the W grains, but the mechanism of their evolution cannot be ascribed to sputtering phenomena due to the low energy of the impinging ions (about 40 eV with a sputtering threshold of 200 eV for D on W) [13,14]. A possible explanation made by Xu et al.[15] is related to the development of a stressed amorphous layer 30 nm thick due to supersaturation of W surface because of the D flux, but this theory lacks direct experimental evidence. Jia et al. [16–18] studied PCW exposed to D plasmas in Pilot-PSI by means of focused ion beam (FIB) and transmission electron microscopy (TEM) proving the existence of subsurface structures beneath the surface nanostructures. It was found that the surface nanostructures on W induced by low energy D plasma were mainly due to two reasons:

1. For W grains presenting the ⟨1 1 1⟩ crystallographic direction, subsurface nano-sized bubbles are formed and induce nano-scale blistering of the surface, resulting in ordered nano-scale surface morphology.

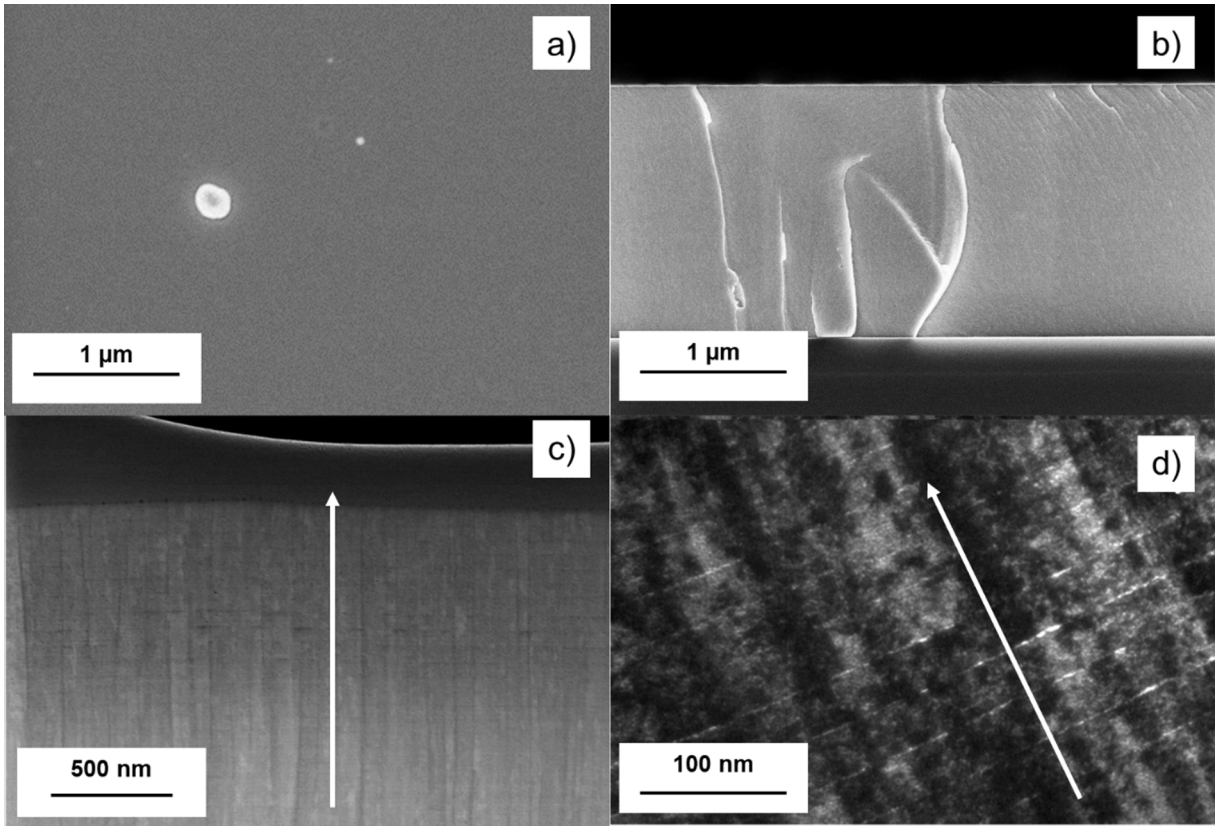

Fig. 1. Pre-exposure morphological characterization of amorphous W (a-W): (a) SEM plain view, (b, c) SEM cross section, and (d) TEM cross section analyses. The white arrows in figure (c) and (d) represent the film growth direction.

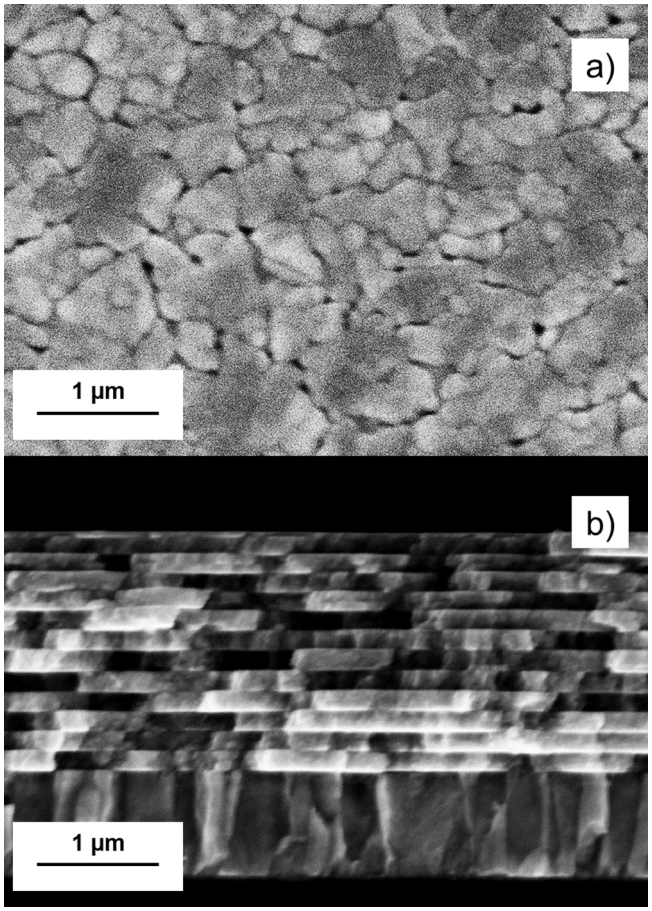

Fig. 2. SEM analysis of the annealed a-W samples in (a) plain and (b) cross section views.

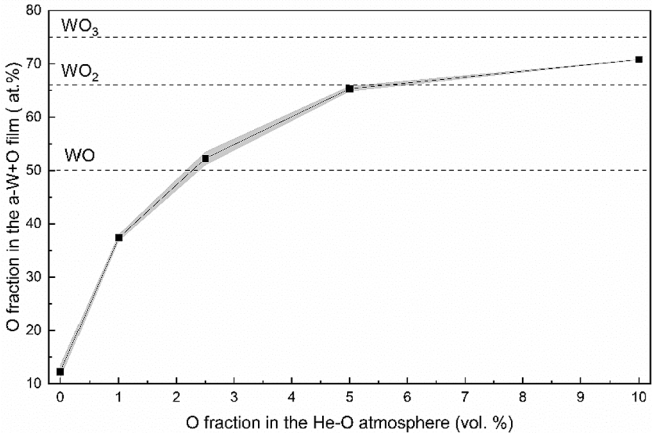

Fig. 3. Oxygen uptake in the a-W films, detected by EDXS, as a function of the oxygen fraction in the He-O atmosphere during the deposition process. Shadowed area represents the uncertainty of the measurement.

2. On other W grain directions, mainly ⟨1 1 0⟩, an oxide layer of about 30 nm thick is found. In this case the hypothesis is that due to the low sputtering threshold (18 eV), this is sputtered by low energy D particles, resulting in the ordered nanostructures on the surface that, in turn, depend on the crystalline orientation of the underlying W grain.

Despite the significant progresses made in understanding the formation of SNs, the role of crystallinity of the substrate as well as the contribution of W oxide must be clarified. Coatings that reproduce the redeposits found in nowadays tokamaks have already been exposed to the low-flux GyM linear plasma device [19] and to the high-flux Pilot-PSI [20]. Both works showed the formation of SNs and blistering on the various coatings, despite the substantially different exposure parameters, namely flux, fluence and impinging ion energy. A similar investigation with an intermediate-flux device keeping a few exposure conditions fixed could help understanding the physical phenomena behind these observations.

In the present work, exploiting the features of Pulsed Laser Deposition (PLD), and its pulsed regime, we deposited on PCW two kind of W coatings, named amorphous (a-W) and porous W (p-W), that exhibit a multi-layered W structure and whose features mimic the ones of redeposited W layers present in tokamak:

- a-W: compact films with high number of defects, such as dislocations and vacancy clusters that determine a lower density (12 g/cm^3 instead of 19 g/cm^3) and crystallite size of few nm (amorphous structure) [21] while the oxygen amount can vary between 10% and 75% [22]. Such coatings resemble, in terms of the number of defects, morphology and structure, some of the deposits found in present-day tokamaks in regions near the strike-point at divertor targets such as first mirrors [23]. In addition, a-W coatings were also annealed to investigate the role of temperature and growth of W grains.
- p-W: porous films characterized by a porous open morphology that determines remarkable decrease in density compared to PCW and poor crystallinity, the oxygen amount is usually 50% [24]. Such kind of coatings are like those found in recessed regions not directly in contact with the plasma.

The samples were exposed to D plasmas in the medium-flux linear machine PSI-2 in divertor relevant conditions at different fluences. D retention and SNs development were assessed and related to the structure, morphology, void distribution (thanks to dedicated TEM analyses) and composition of the different W coatings.

In addition, the study of a-W layers that present an amorphous structure with a variable oxygen content and once annealed, crystalline grains with ⟨1 1 0⟩ orientation, allows investigating the formation dynamics of SNs highlighting the role of W crystallinity and presence of oxygen at the W surface.

Experimental

Deposited samples

Multi-layered W samples were produced using a PLD deposition system. Nanosecond laser pulses at the wavelength of the 2nd harmonic of a Nd:YAG laser ($\lambda = 532$ nm, pulse duration 5–7 ns, repetition rate 10 Hz) are focused on a W target (purity 99.9%). The laser spot is about 9.2 mm^2, pulse energy is 815 mJ and laser fluence on the target 15 J/cm^2. The species ablated from the target expand in a high-vacuum chamber (base pressure of 10^{-3} Pa), where different ambient gases (He, mixed He-O or Ar) are introduced. The expanding species are collected on grounded rotating silicon (1 0 0) substrates (size 2.5 mm × 2.5 mm) or on polycrystalline W plates (PLANSEE, 99.96% purity, 1 mm thick) containing micrometer-sized grains and mechanically polished until mirror finish. In both cases, the obtained films are 1 μm thick. The substrate is 60 mm away from the target at room temperature. For every deposition the first layer is made of 150 nm of dense nanocrystalline W that acts as adhesion layer.

- A He pressure of 70 Pa is chosen to induce the growth of amorphous W (a-W) as reported in [21].
  - o A He-O atmosphere was set, by adding a proper O flux (0 – 10% of total flux), to induce the deposition of a-W with an increasing oxygen content called a-W + O films.

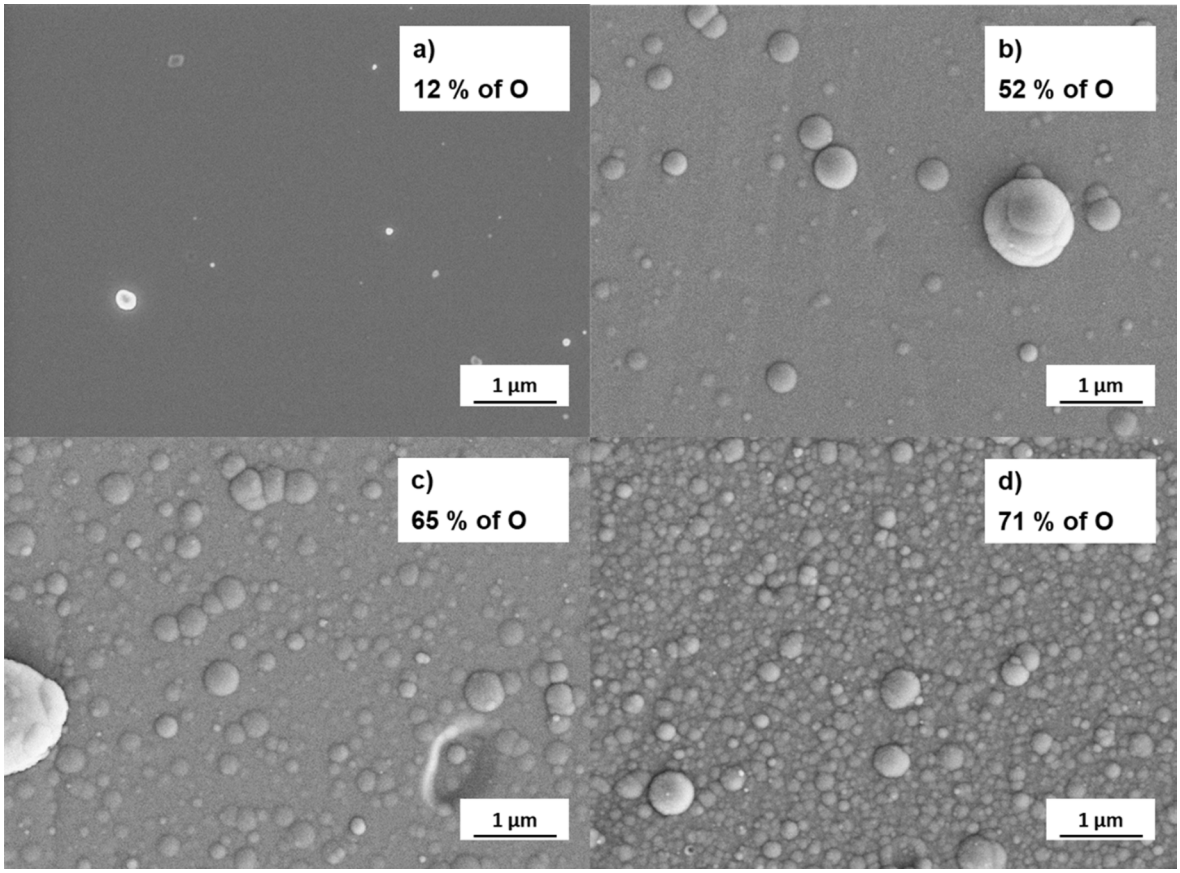

Fig. 4. SEM plain view of a-W samples with increasing oxygen content from 12% to 71% (a-d).

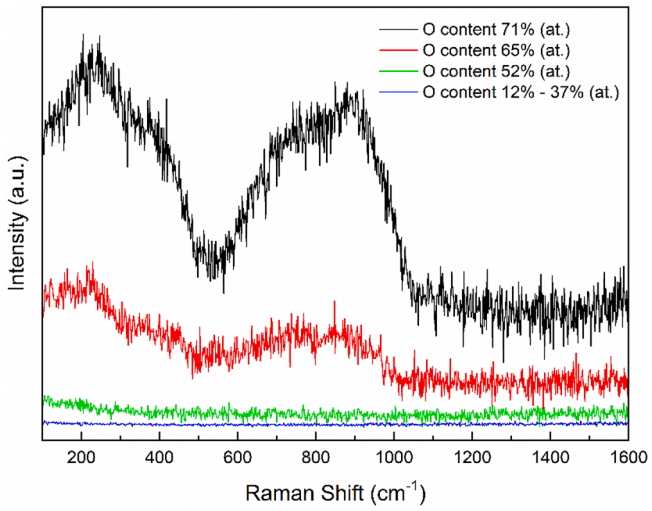

Fig. 5. Raman analysis of a-W samples with different oxygen content.

- o Some a-W films were subsequently annealed in vacuum at 750 °C for 1 h to induce the crystallization of the W film (a-W ann. samples) as reported in [25].
- An Ar pressure value of 50 Pa is set to grow porous W (p-W) [26].

The films were characterized with a Zeiss Supra 40 field emission scanning electron microscope (SEM, accelerating voltage 5–7 kV). To determine the film composition, energy dispersive X-ray spectroscopy (EDXS) is performed using an accelerating voltage of 15 kV, to excite Kα and Mα electronic levels of oxygen (O) and W, respectively. Kα of cobalt is used for system calibration. This kind of technique gives only preliminary results due to the known uncertainties related to the physic of electron-matter interaction. Nevertheless, this technique is useful to detect relative variations between the different samples as well as prior and after exposure. A detailed analysis of the structure and morphology of the coatings was performed by means of FIB-SEM Hitachi 2100 with an accelerating voltage of 30 kV and Ga ion source and subsequent TEM Jeol 1200 with an accelerating voltage of 120 KV. The structure and crystallinity of the resulting films have been assessed also by X-Ray Diffraction (XRD), using a Panalytical X'Pert PRO X-ray diffractometer in the θ/2θ configuration. Kα radiation has been used, current at the anode is 40 mA with a tension of 40 kV. The investigated range is 20–90°. Presence of oxygen compounds has been assessed by micro-Raman measurements, with a Renishaw InVia spectrometer equipped with an Ar + laser (λ = 514.5 nm), a 1800 g/mm grating and an edge filter with cut at 100 cm^{-1}. The laser operates at 1mW continuum power through a 50 × objective to avoid any local material modification.

PSI-2 exposure

All the deposited W samples were exposed at the linear plasma generator PSI-2 at FZJ. The samples were exposed to deuterium plasmas with the features reported in Tables 1 and 2. In all the depositions the substrate was isolated (no intentional bias was applied) and thus reached a floating voltage. The energy of the impinging ions was evaluated being 5 times the electron temperature in eV, the considered values are in agreement with experimental measurements made on PSI-2 [27].

The D content was assessed by Nuclear Reaction Analysis (NRA) using the reaction D (^{3}He; p)^{4}He. The sample is placed in a vacuum chamber and is exposed to a ^{3}He beam with a fixed kinetic energy. The intensity of the resulting emitted radiation is recorded by two different

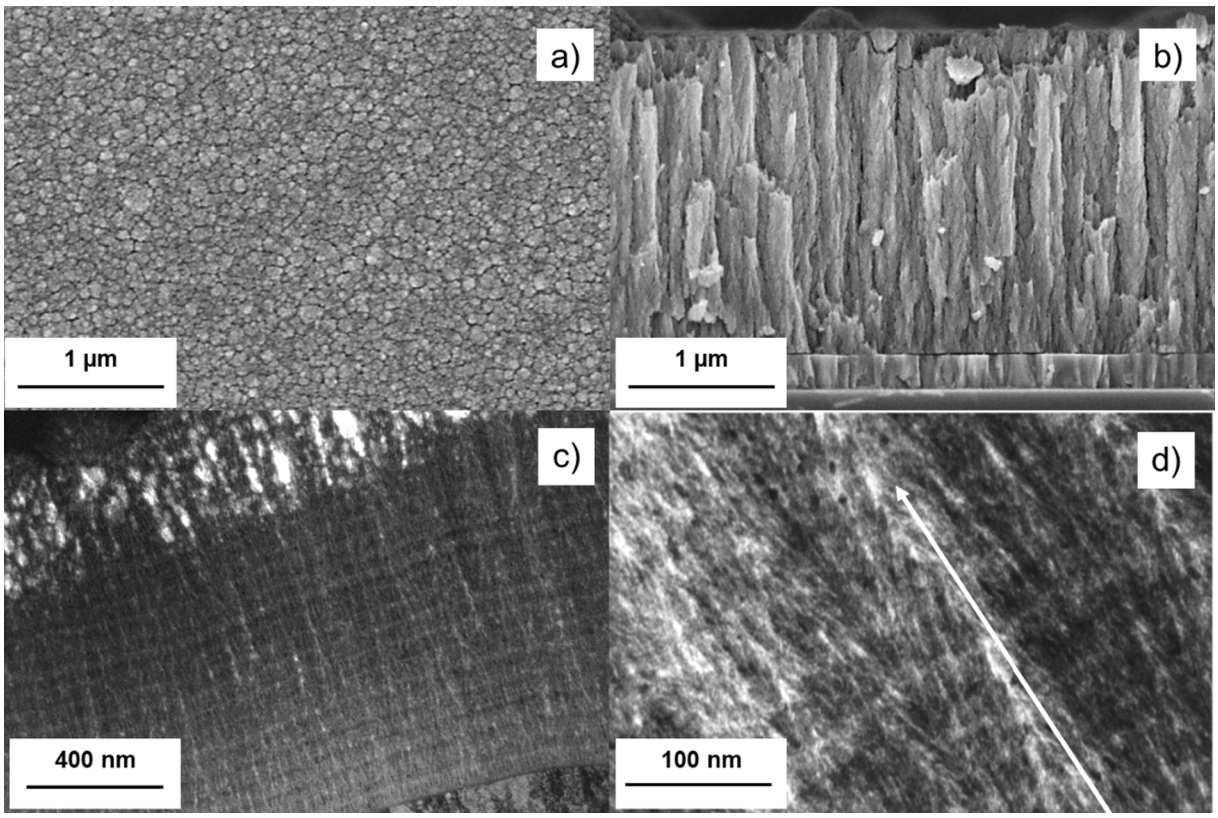

Fig. 6. Pre-exposure morphological characterization of porous-W (p-W) samples: (a) SEM plain view, (b) SEM cross section and (c-d) TEM analysis. The white arrow in figure (d) represents the film growth direction.

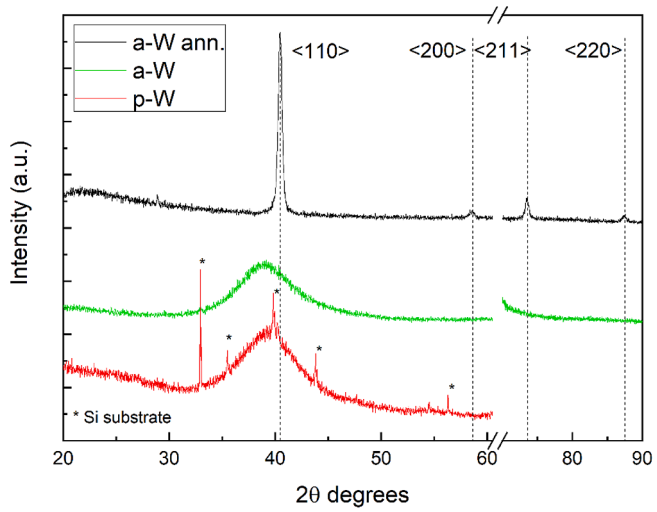

Fig. 7. XRD analysis of a-W, annealed a-W and p-W samples.

detectors placed at a scattering angle of 165°. The incoming beam energy was set to 3.5 MeV to have an overall depth of D concentration. The SIMNRA software [28] was used to interpret the spectra acquired.

Results

Characterization of the coatings before PSI-2 exposure

In Fig. 1 the results of SEM analyses of amorphous W samples are reported. As it can be seen (Fig. 1 a-b) this kind of W exhibits a featureless morphology both in plain and in cross section. Thanks to the SEM/TEM analysis (Fig. 1 c-d) it is possible to detect a stratified structure made of 30-nm thick W layers deposited perpendicularly with respect to the growth direction (indicated by the white arrow). The white spots visible in Fig. 1d that have been identified as voids, that are accumulated at the boundaries between the single layers. The development of this very particular kind of structure is probably related to the pulsed regime of PLD in combination with a relatively low kinetic energy of the species arriving at the substrates (compared with the "in vacuum" case) that is high enough to induce the formation of a compact film but not enough to induce the formation of crystallites, more details are reported in [21]. This kind of layered structure resembles the W-O redeposited layers found in AUG redeposits [4]. Both AUG redeposits and the a-W layers present an sub-layered morphology where the sub-layer thickness is in the range 30–200 nm. Both layers are made of W and O and their structure is amorphous. In addition in AUG redeposits the presence of layers of light elements such as boron and carbon is found as well as the presence of pores several microns long. Boron and carbon are not present in the deposited coating but they could be added during the deposition process by ablating boron targets to mimic even better the features of the redeposited coatings found in tokamaks.

Fig. 2 shows the results of SEM cross section analyses from annealed a-W samples. The annealing conditions determine a crystallization of the amorphous W film that now appears to be composed of grains of 100 – 500 nm wide. From the cross-section analysis, it is possible to see that the multilayer morphology is still present, and each W layer seems to crystallize independently leading to the formation of a multilayer structure that can be identified also by SEM.

In Fig. 3 the oxygen uptake in a-W films, detected by EDXS, as a function of the fraction of oxygen present in the He-O atmosphere is displayed. As visible from the graph varying the O fraction between 0 and 10% it is possible to induce oxygen retention in the range of 12–70%. A minimal residual O content of 12% is unavoidably present in this kind of coating due to the deposition dynamics of PLD [21].

Table 3
Features and deposition conditions of the grown samples before exposure.

Name	Dep. gas	Atmosphere composition (% vol.)		Dep. pressure (Pa)	T ann. (°C)	Morphology & structure	O content	
							EDX	IBA [24]
a-W	He	100	0	70		compact, layered, horizontal voids, amorphous	12%	25%
a-W ann.	He	100	0	70	750	compact, layered, nanocrystalline	8%	
a-W(O)	He, O	99	1	70		compact, layered, horizontal voids,	37%	
	He, O	97.5	2.5	70		amorphous	52%	
	He, O	95	5	70			65%	
	He, O	90	10	70			70%	
p-W	Ar	100		50		porous, layered, vertical voids, amorphous	55%	62.5

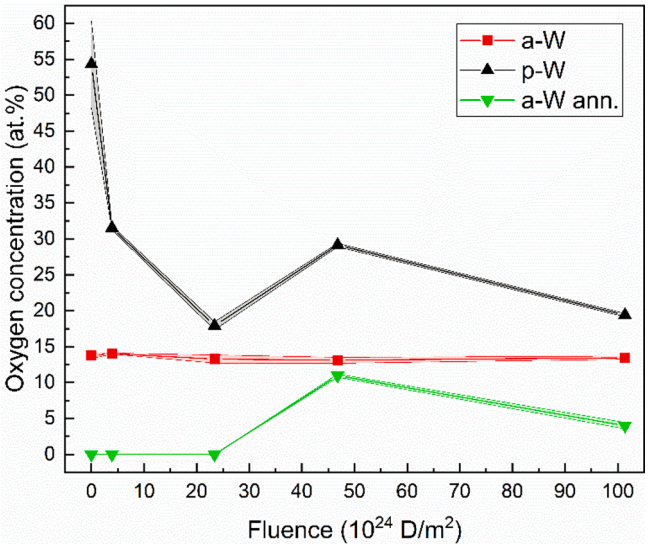

Fig. 8. Oxygen concentration in the three kinds of samples as a function of exposure D fluence. Shadowed area represents the uncertainty of the measurement.

In Fig. 4 the corresponding SEM plain view images are visible. The increase of the oxygen content does not alter the compact morphology of the film but results in the formation of many cauliflower structures with a width of 100 nm and the number density increasing accordingly with the oxygen content.

The outcomes of Raman analyses of a-W coatings with varying O contents are visible in Fig. 5. This characterization allows to extract information on the growth of W oxide in the a-W coatings increasing the O uptake. As visible in the Figure, Raman spectra does not show any peak for oxygen contents up to 52%. In this kind of coatings, oxygen is probably trapped in the nanovoids or stabilized by defects in the W lattice [29]. For W coatings with a higher O content, Raman spectra show the appearance of bands that are compatible with the formation of an amorphous and thin superficial W oxide probably related to the increased roughness of the W surface more than a massive oxidation of the whole coating.

In Fig. 6 morphological analysis, performed by SEM and TEM, of porous W is shown. As also shown in [24] porous W presents a very rough morphology (Fig. 6a), the film appears to be constituted of porous tree-like columnar grains (as referred in [30]) 100 nm wide with heights corresponding to the film thickness (Fig. 6b). Thanks to the TEM analysis, it is possible to notice again the presence of a multi-layer structure that also in this case depends on the pulsed regime of the deposition technique (Fig. 6 c). Similar structures have been observed after experimental campaigns at WEST due to the synergic effect of W, O and B redeposition [9]. Also, in this structure many voids are present, but differently from the a-W case, the voids are distributed along the growth direction giving a completely different scenario. In this kind of W, that is deposited at low W energy, the EDXS analysis shows an oxygen content of about 55% due to the porous morphology of the surface. Raman analysis, not shown, reports the formation of a superficial W oxide.

In Fig. 7 the outcomes of XRD analyses from a-W, annealed a-W and p-W samples are reported. As already stated, both a-W and p-W structures exhibit an amorphous structure. In fact, in both cases only a broad band around 40° is visible. Instead, annealed a-W diffractogram shows the presence of well-defined peaks in the position related to metallic W. The most intense peak is the one related to the ⟨1 1 0⟩ direction.

In Table 3 the synthesis parameters as well as the features of the exposed films are reported. In addition to the presented analysis the values related to oxygen concentration can be compared with ion beam analyses (i.e. Rutherford back-scattering and time of flight-elastic recoil detection analysis) performed on W-O samples deposited in the same way. Thanks to this comparison we can see that EDXS analysis underestimates the oxygen concentration in the films. In fact, O% determined by IBA is 62.5% for p-W and 25% for a-W [24].

Characterization of the coatings after PSI-2 exposure

In Fig. 8 oxygen concentration, estimated by EDXS, in the different kinds of samples versus D fluence is reported following their exposure to PSI-2 plasmas. Reference values correspond to zero fluence. It is possible to notice that the O concentration does not vary in a-W samples due to the compact morphology and the homogeneous distribution of O in the thickness of the coating remaining at 15%. Also annealed a-W films exhibit only small variations of O concentration in the range 0–10% the lower amount of O respect to the non-annealed film has to be ascribed to the annealing process. In fact, it has already been reported that annealing of a-W even at moderate temperatures (e.g. 500 °C) results in the migration of O towards the surface with consequent formation of WOx nanowires [31]. The behaviour of p-W is different. Immediately after the first exposure the O content falls from 55% to 30%, increasing fluence it ranges between 20% − 30%. This dynamic confirms that a superficial layer of W oxide was present on this coating and O has been scavenged by the interaction with the reducing atmosphere of D plasma. Fluctuations of O content in a-W ann. and p-W could be related to post-oxidation phenomena of the metallic surface since the EDX analyses were made after exposure of samples to air.

In Fig. 9, SEM plain view of the surface of a-W exposed at different fluences is shown. Up to 2.3×10^{25} (D/m^2) only small corrugations of the surface are visible, but above 4.7×10^{25} (D/m^2) a defined nano-structured morphology is clearly visible. Randomly oriented string-like structures a few nm wide and 10 nm long can be clearly seen.

In Fig. 10 the development of the surface structures is shown in the case of annealed a-W. As in the previous case, slight modifications occur for a D fluence up to 2.3×10^{25}. When the fluence reaches the value of 4.7×10^{25} the nanostructures are clearly visible. They are strait and clearly limited by the grains of the film, this behavior has already been reported in the case of bulk crystalline W. Here, for the first time, it is possible to show that the same dynamics is reproduced also at the

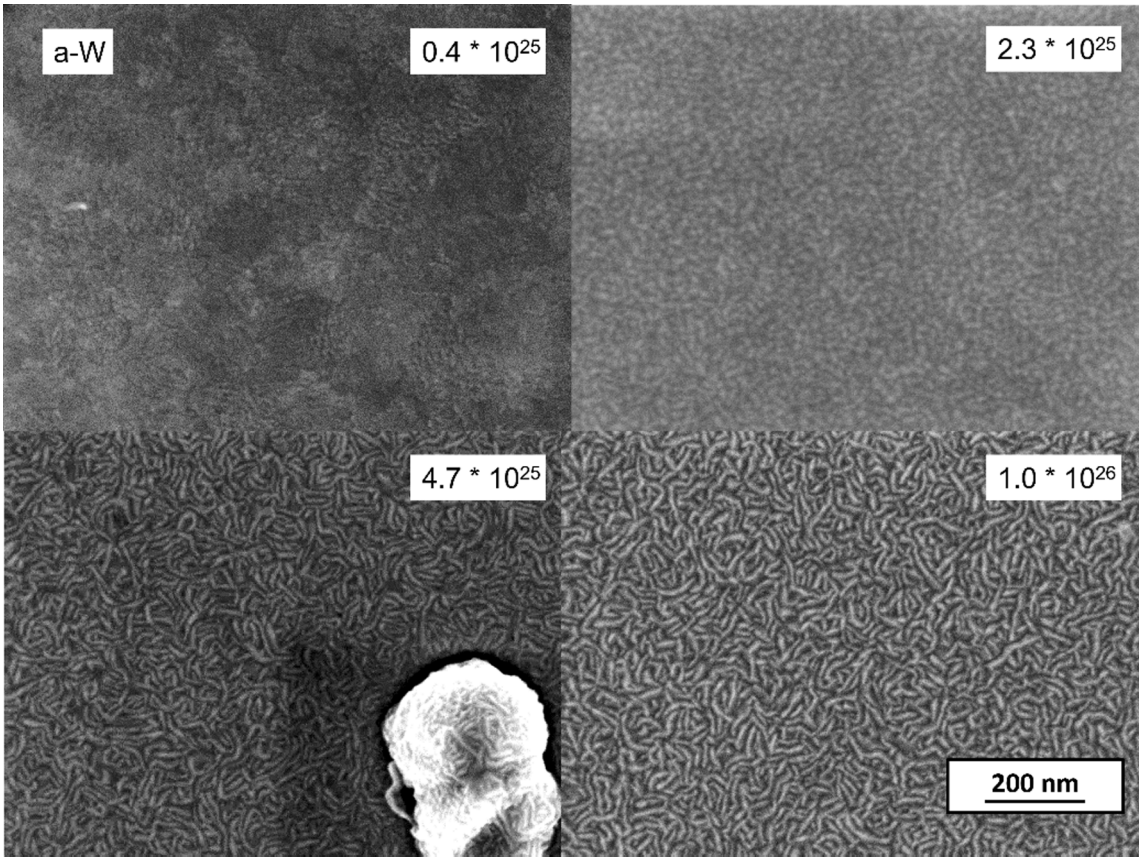

Fig. 9. Post-exposure SEM plain view of a-W samples as a function of D fluence.

nanoscale. At higher fluences the lamellar structure is preserved but the features of the lamellae are different. They are thicker and more grains seem to show a featureless structure.

In Fig. 11, SEM plain view images of the surfaces of exposed a-W samples containing different amounts of O are presented for the highest applied D fluence. It is possible to see that the presence of a remarkable amount of oxygen in the W coating alters the features of the produced nanostructures. In fact, in the present case, nanostructures appear much straighter and longer with respect to the ones made with low O amounts. Increasing the O content does not change the morphology, but the film exhibits many small cracks.

SEM plain view analysis of the porous W shows how its rough morphology is affected by the D fluence. In samples exposed at fluences from 0.4×10^{25} D/m^2 to 4.7×10^{25} D/m^2 a sputtering of the p-W surface is observed: the exposed surface has become cleaner, and the single aggregates start to appear. The proposed view agrees with the O trend in this kind of sample. The oxidized surface is chemically scavenged by D. At very high fluences it is possible to appreciate the formation of nanostructures on the nanometric domains.

In Fig. 13, D retention versus D fluence for the different W samples is shown. All the exposed samples present a peculiar sigmoid trend, with a low increase in D retention for fluences under 2×10^{25} D/m^2 followed by a sudden increase in the range $2–5 \times 10^{25}$ D/m^2. In addition to this, it is possible to see how the structure of the film influences the retention properties. Deuterium retention in a-W is higher compared with the one of p-W. The former retains 10^{21} while the latter 10^{20} for fluence of 10^{26} despite the higher porosity of the p-W film. It is interesting to note that the amount of D retained is not so much influenced by the presence of O except in very high concentrations. On the other side in annealed a-W D retention is about 10^{18} D/m^2 with a slight increase with fluence.

Discussion

Nanostructures development

With the aim of understanding which are the main D plasma parameters affecting the formation of surface nanostructures (SNs), Fig. 14 plots the fluence (D/m^2) against the flux in various deuterium irradiation experiments conducted in PlaQ [32–34], GyM [19], PSI-2 [35] and Pilot-PSI [14–18,36] considering an incident ion energy of about 40 eV. The error bars are estimated being 25% the typical uncertainty of Langmuir probe techniques usually used to characterize the D flux [37,38].Closed markers represent the cases where the SNs were formed, while open markers the cases without observations for nanostructure formation. In Fig. 14 squares represent the PCW whose data come from literature while circles, diamonds and triangles represent a-W, a-W ann. and p-W respectively whose features are described in [14] for the exposures at GyM while the ones exposed to PSI-2 are the object of the present work and have been presented in the previous section. Looking at Fig. 14 it can be noted that the SNs formation starts above a certain fluence value (about $3–5 \times 10^{25}$ D/m^2) regardless of the value for the impinging flux, ranging over 4 orders of magnitude, and the specific plasma machine. A remarkable exception is constituted by a sample exposed by Xu et al. [14] in Pilot-PSI at a fluence of about 8×10^{26} D/m^2 but with an intentionally reduced bias of 5–6 eV (as indicated in the Figure) where SNs does not take place due to the low energy of the impinging species. Conversely SNs formation was found in GyM at low fluence but applying a bias ranging between 100 and 300 eV (also indicated in the Figure) [19].

In general, nanostructured coatings follow the trend observed with PCW with some exceptions that we found in p-W, see Fig. 12. Nanostructures on a-W start to form at 2.3×10^{25} D/m^2 and are completely evolved at 4.7×10^{25} D/m^2 with no further evolution. The absence of a

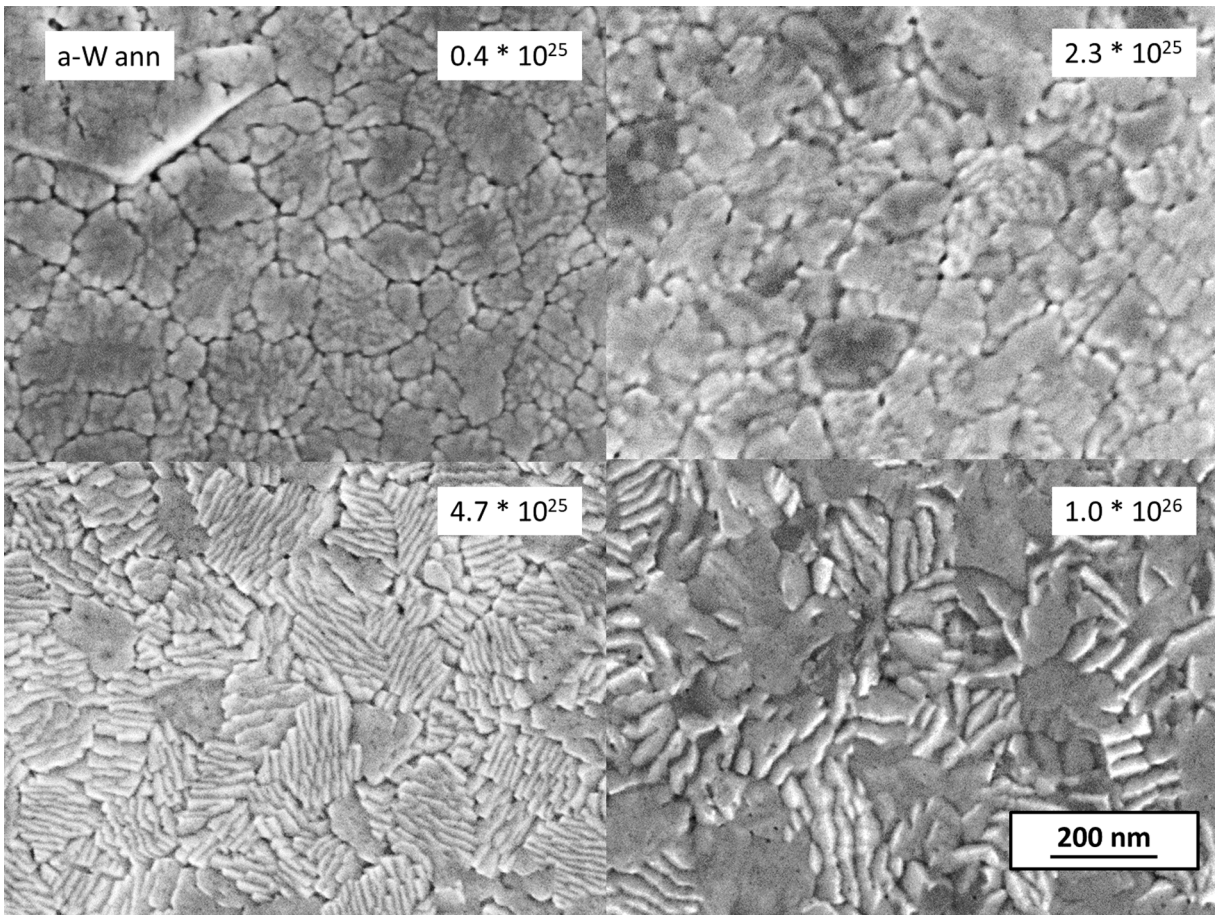

Fig. 10. Post-exposure SEM plain view of annealed a-W samples as a function of D fluence.

"canonical" shape (i.e. lamellar, triangular, or spongy) is a remarkable clue about the importance of crystalline structure in the underlying W surface. In this case the amorphous surface seems "unable" to determine the shape of the SNs. On the other side, a-W exposed to high flux Pilot-PSI plasma (flux 1.4 × 20^{24} D/m^{2}s^{-1}, fluence 2.5 × 10^{26} D/m^2) determines the formation of much more regular structures, although not as the ones formed on PCW [20]. Since in both the exposures the substrate temperature is set at 200–300 °C the detected differences can be ascribed to different D fluxes in the two experiments.

As in the case of a-W, also annealed films exhibit the formation of nanostructures, see Fig. 10. The fluence range is the same as for a-W and confirm that the fluence of 4.7 × 10^{25} D/m^2 can be considered as a trigger value. The crystallinity of the W grains, oriented mainly along the ⟨1 1 0⟩ crystallographic direction, see XRD analysis in Fig. 7, determines the formation of lamellar or jagged structures as already shown on PCW [15,18]. Interestingly we note that in this case the features of the nanostructures are related to the fluence. In fact, going from 4.7 × 10^{25} D/m^2 to 1 × 10^{26} D/m^2 results in a coalescence of the lamellae formed on the different grains. This kind of behavior has not been observed before.

Not only the crystallinity of the W grains determines the shape of SNs in a-W films, but at the highest D fluence, when the amount of oxygen reaches 50%, we observe the formation of new kind of SNs that are no more randomly oriented string-like structures but appear much straighter and are more aligned, see Fig. 11. Increasing the amount of oxygen over 50% does not significantly change the morphology of the SNs. As highlighted in Jia et al, the presence of a thin layer of W-O is fundamental in determining the features of the SNs [18]. But in that experiment the W-O layer is grown on crystalline W and the shape of the SNs is always in connection with the crystalline orientation of the underlying W grain. In our case no crystalline matrix is present and thus, the SNs shape is determined only by the interaction of D with the W-O layer. In the same work it is reported that the exposure of thermally grown W oxide to D flux does not result in the formation of any kind of SNs. Thus, we can infer that the new morphology is related to the presence of an amorphous W-O surface, as detected by Raman analysis see Fig. 5, with high amount of oxygen (>50%). The importance of an amorphous layer is also assessed by Guo et al. [39]. Using TEM analysis of thin W monocrystalline layers, they detected a severe distortion of W surface exposed at 5 × 10^{21} D flux leading to the formation of amorphous and nanocrystalline regions in monocrystalline W. The appearance of such distorted W surface seems to be a necessary condition for the SNs formation.

The observations made in the present work confirm the hypothesis made by Jia et al. [16,18] of an important contribution of the W-O system in the formation of SNs. In fact, referring to the case of PCW, the thickness of native tungsten oxide is usually less than 5 nm [40], and the typical height of SNs found on ⟨1 1 0⟩ grains are in the same thickness range. In addition, SNs of PCW appear also at low fluences but with a high energy of the impinging particles (100–300 eV) [19]. In this case, the energy of the impinging particles leads to a higher sputtering rate that can compensate the lower D fluence.

It's worth to note that the exposure of a-W + O films was performed at an higher temperature respect to the other films 298 °C instead of 201 °C respectively. Also substrate temperature could play a role in the formation of this new kind of nanostructure. But the exposures reported in literature are performed form 100 °C up to 800 °C [13–17]. In every case the usual SNs, lamellar sawtooth and spongy, are formed. At 670 °C in addition to the SNs nanometric pinholes start to appear not correlated to the SNs. Thus, the role of temperature in the investigated range, seems

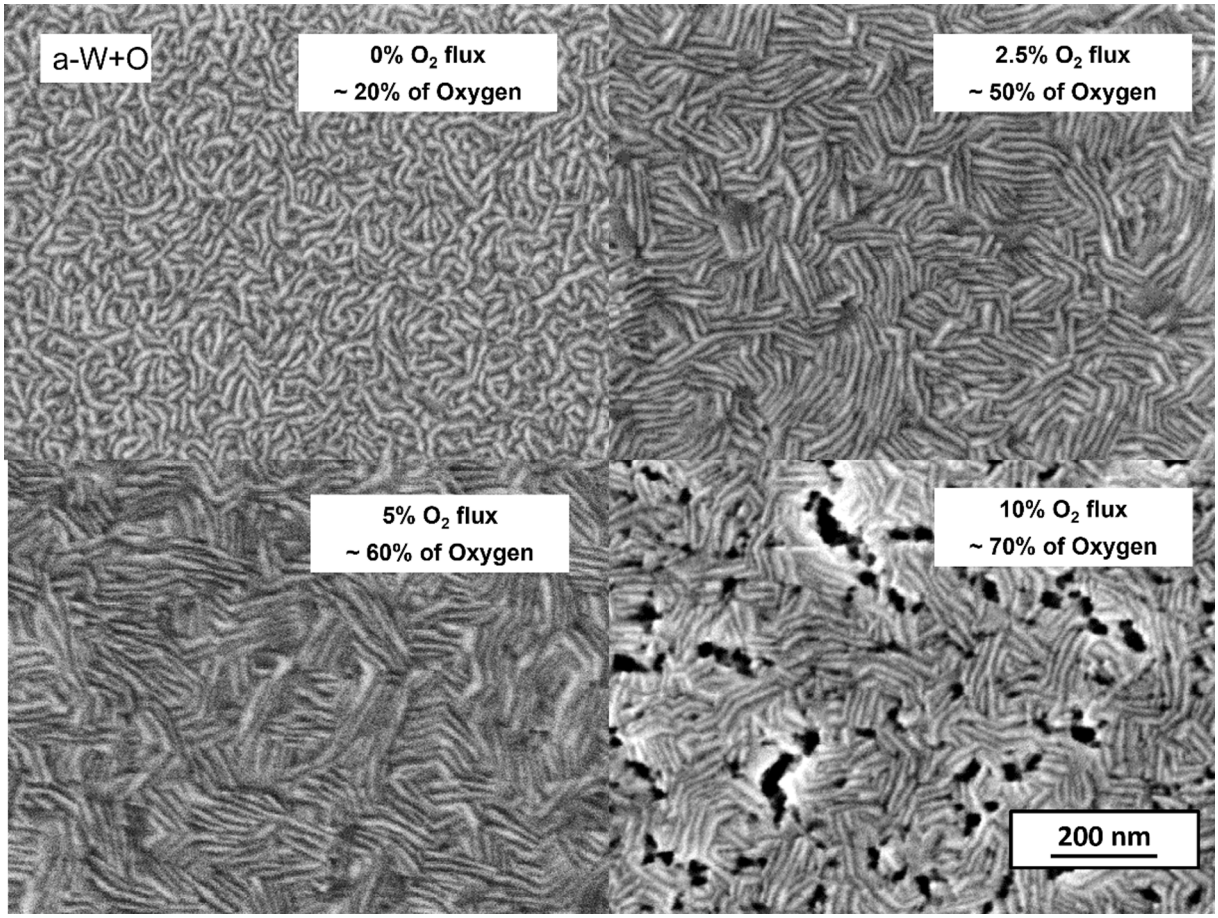

Fig. 11. Post-exposure SEM plain view of a-W samples with different amounts of oxygen content. The D fluence is fixed to 1.0×10^{26} D/m^2 for all samples at T_{surf} = 298 °C.

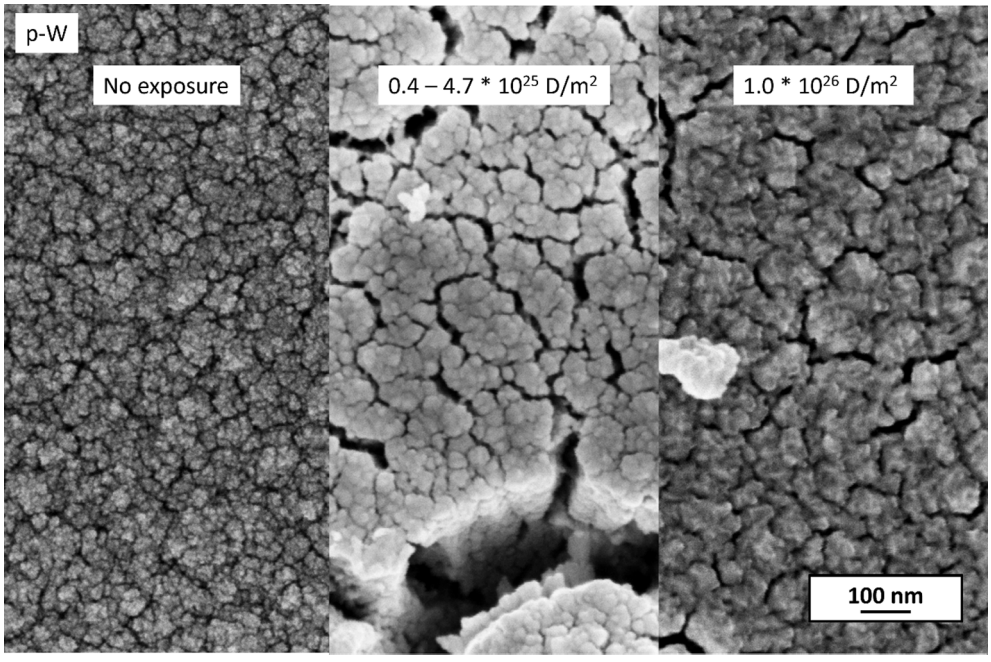

Fig. 12. Post-exposure SEM plain view of p-W samples as a function of D fluence. The interval present in the middle image indicates that morphology is not varying in that D fluence range.

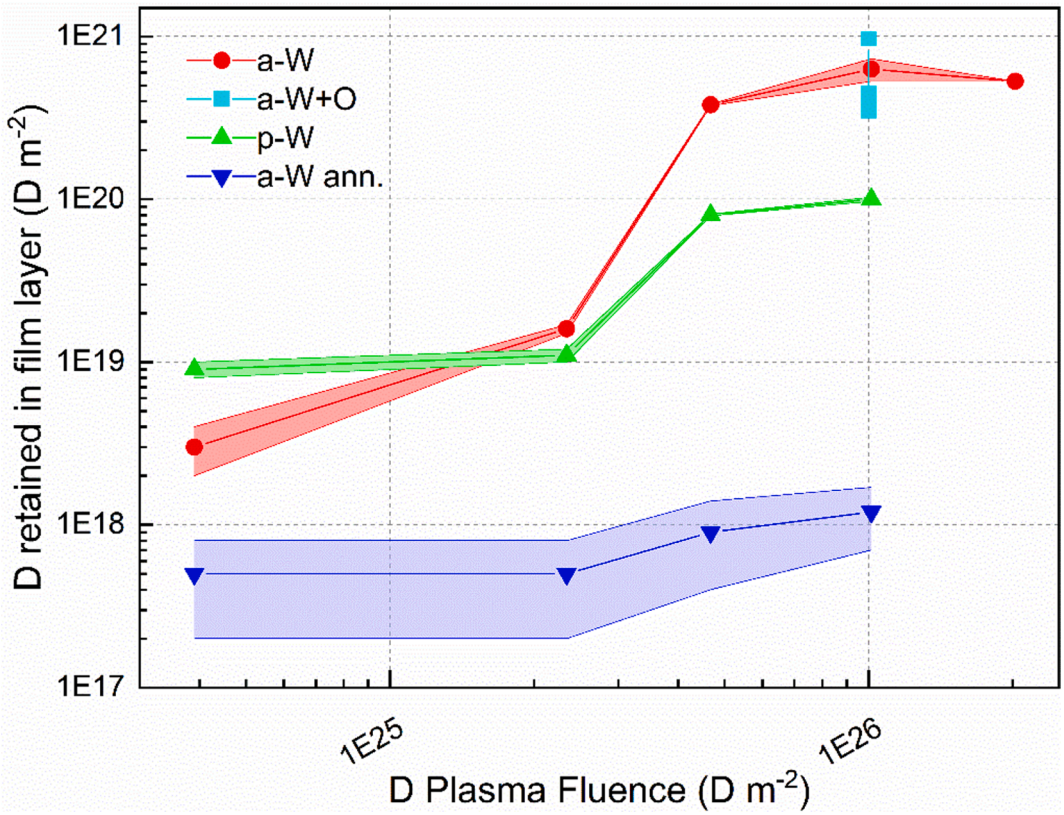

Fig. 13. D retention, detected by NRA, for the different exposed samples as a function of D fluence. Shadowed area represents the uncertainty of the measurement.

to be minimal respect to the role played by oxygen.

p-W films do not show the formation of SNs in the range 0.4 – 4.7 × 10^{25} D/m^2, only a smoothing of the surface takes place. Thanks to the EDXS analysis, see Fig. 8, we can infer that the surficial layer is made by a porous W rich of oxygen that gets chemically eroded by the D flux at the beginning of the exposure, determining a smooth morphology. The same behavior can be found for low flux, low fluence exposure of p-W in GyM [19]. The absence of SNs in this fluence range can be ascribed to the small dimension of the W domains, that are neither crystalline nor enough compact due to the high number of vertically aligned voids in p-W morphology, as visible in Fig. 6. Evidently in such conditions it is not possible to form the stressed W-O layer that is necessary for the formation of SNs due to the high surface to volume ratio of such morphology. Only at high fluences (>10^{26}) a small nano-structuring appears but it is difficult to ascribe it to the previously mentioned formation mechanism of SNs.

Retention properties and trends

As visible in Fig. 13, the trend of retained D versus fluence in log–log representation clearly shows a sigmoidal trend. This fact is very peculiar since it is well known that for W bulk this trend is linear in the temperature range of 107 °C – 370 °C [41,42]. It is known that such trend is affected by W composition as well as impurities in the plasma [43] but a sigmoid trend has not been reported. A similar "latency" in the trend is observed when the D retention of a 3 μm thick layer of W fuzz is investigated as reported by Sakai et al. [44]. Thus we can speculate that the observed peculiar behavior is related to the presence of a micron-thick W layer with features (composition, crystallinity, etc.) significantly different from W bulk.

On the other side it is known that due to the different diffusivity of D in films and bulk the interface can induce the development of blisters. But the number of blisters is very small and they can be detected with statistical significance only with a D fluence of 10^{26} D/(m^2s) and only for a-W (not shown). They are relatively small (about 20 um) and few compared with the ones found after exposure of a-W to high flux plasma [20]. Thus we can imagine that due to the relatively low fluence the amount of stored D at the interface is minimal respect to the ones stored in the films.

Among the different kind of W layers investigated a-W retains the highest amounts of D thanks to its compact morphology combined with an amorphous crystalline structure. In addition, due to the presence of voids distributed parallel to the surface, there are no preferential ways for D diffusion and recycling. The dependence of retention on the crystallite order is also confirmed by earlier studies where W films with a crystalline dimension of 2–15 nm, deposited by Pulsed Laser Deposition, were exposed to a D flux in Pilot-PSI: they exhibited D retention almost one order of magnitude higher than polycrystalline W (0.96–2.1 × 10^{21} D/m^2 vs 8.6 × 10^{19} D/m^2) [20]. Similar results have been obtained after the exposure of various W coatings (prepared with different techniques) to the plasma of PLAQ. It was found that all types of coatings, exhibiting a nanocrystalline structure, show higher D concentration compared to PCW [45]. A lower diffusivity of N in a-W films exposed to D-N plasma in GyM compared to nanocrystalline W has also been reported [46]. It is interesting to note that oxygen, although present in a remarkable amount in the film (12–70%), plays almost no role in D retention.

When these kinds of coating are annealed, retention in the layers drops to the levels of the reference PCWs. It's worth noticing that also annealed a-W retains the multi-layered structure as reported in Fig. 2. Thus, the void distribution present at the interface of the sub-layers does not seem to play a determinant role in increasing D retention. What is significantly affecting D retention is the restoration of the crystalline order in the W sub-layers where the crystallite size grows from about 3 nm to 20 nm.

Porous coatings show a different dynamic compared to a-W. At low fluences, D retention is higher than a-W but at high fluences is one order

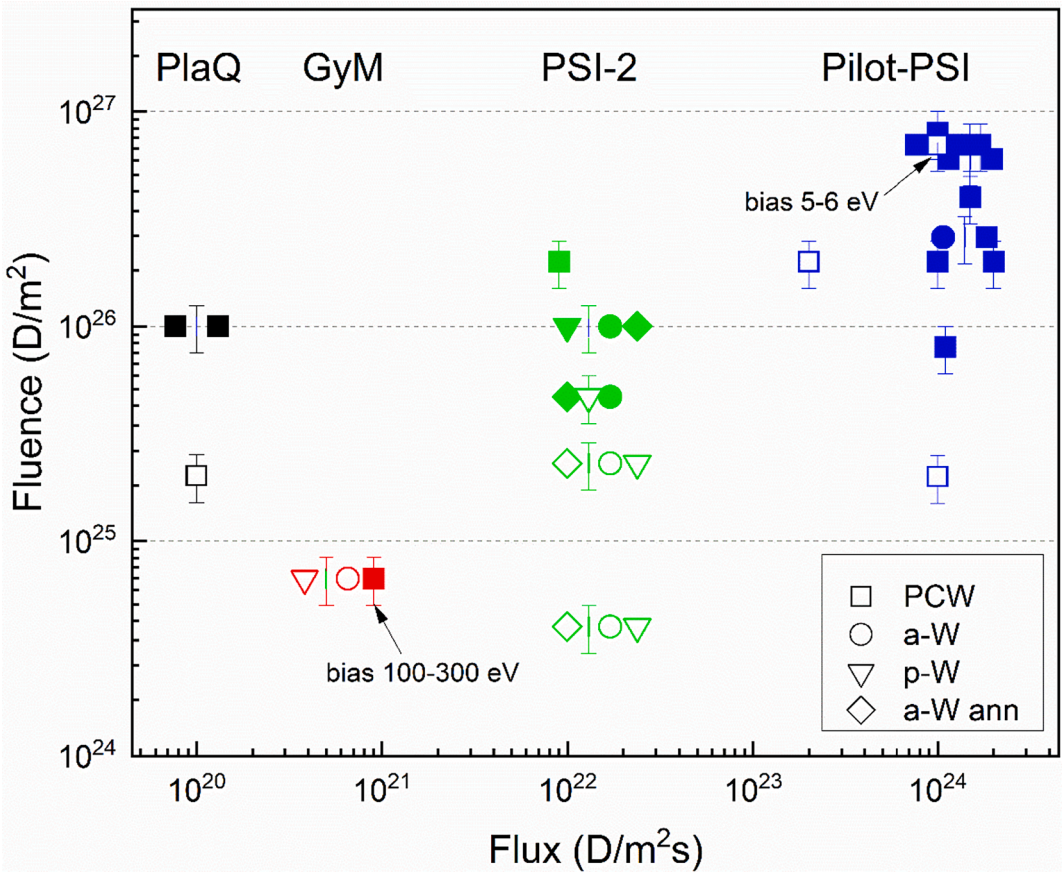

Fig. 14. Overview of D-plasma exposure of different W samples in PlaQ, GyM, PSI-2 and Pilot-PSI linear plasma devices, as a function of D flux and D fluence. Closed markers represent the cases in which the SNs were formed, while open markers represent the cases where the nanostructures were not observed.

of magnitude lower compared to the ones of a-W. In this case, the porous morphology, that results in a distribution of voids perpendicular to the surface as well as a higher surface area, determines an increased recycling of D, resulting in a lower retention with increased D fluence. Also, this behavior has been found in literature: p-W coatings exposed to MAGNUM exhibit a different distribution, in the film volume, of retained D compared to crystalline compact films [47,48]. Similar results have been found also when other gas species with respect to D were used. As reported by Mateus et al., after implantation experiments p-W allows retention of a significant He amounts [24]. Nevertheless, also a fast release takes place, and five months after implantation most of the implanted He has been released from the surfaces. For comparison, the compact morphology of a-W films retains higher amounts of He five months after exposure. Finally, is interesting to note that retention in p-W films is very similar to the ones reported in 3 μm thick W fuzz, probably due to the similarities in layer morphology [44]. But if exposed to "dirty" D plasmas (as in tokamaks, also with impurities) porous W coatings could exhibit higher D retention, compared to the compact ones. In this case, because of larger effective surface area, formation of co-deposited layers with high D retention ability could be promoted.

Conclusions

In the present work we exposed to divertor relevant D plasma, in PSI-2, different kinds of W layers resembling the ones found after campaign in tokamak, namely amorphous W samples full of defect as well as porous W films. D retention as well as nanostructure formation were investigated.

After a review of the experiments related to the formation of SNs, we proved that the appearance of such nanostructures on the exposed W surface depends critically on the D fluence with a threshold of about 3–5 $\times 10^{25}$ D/m^2 considering an energy of D ions of 40 eV. At the same time no dependence on ion flux has been found at least in the range 10^{20}–10^{24} D/m^{2}s. In the few cases reported in this paper, the impinging ion energy seems to influence SNs formation, reducing fluence threshold at higher impinging energies and increasing it at lower ones. However, further experiments are needed to better clarify this aspect.

We found that the shape of the surface nanostructures is determined by the crystallinity of the underlying W film and by the exposure conditions. For nanocrystalline W films we found lamellar structures that coalesce with increasing D fluence. Instead, on amorphous W films no lamellas were formed but a new random string-like shape. In addition, increasing the amount of oxygen in the W layer, without affecting crystallinity, results in an evolution of the shape of the SNs in straight parallel lines with acute angles showing the importance of such amorphous W-O layer. The presence of a porous structure morphology hinders the formation of surface nanostructures.

In general, we found that D retention shows a peculiar trend with fluence probably due to the presence of a layer of a nanostructured W. Its amount is enhanced by the presence of amorphous structure and open morphology. Compact amorphous layered W films exhibit higher D retention (3 orders of magnitude) compared to crystalline W. When the amorphous W is annealed, retention returns to the standard values of PCW regardless of the presence of a layered structure parallel to the substrate. Porous W, thanks to the high surface to volume ratio and the presence of void distribution along the growth direction, favors higher recycling and thus limits the D uptake during exposure. The presence of O, in the investigated coatings, seems to have little effect on D retention.

CRediT authorship contribution statement

D. Dellasega: Writing – original draft, Writing – review & editing, Conceptualization, Methodology, Investigation, Formal analysis, Visualization. **G. Alberti:** Writing – review & editing, Formal analysis, Visualization. **E. Fortuna-Zalesna:** Investigation, Writing – review & editing. **W. Zielinski:** Investigation. **A. Pezzoli:** Conceptualization, Investigation, Formal analysis. **S. Möller:** Investigation. **B. Unterberg:** Supervision. **M. Passoni:** Supervision, Funding acquisition, Writing – review & editing. **A. Hakola:** Supervision, Writing – review & editing, Project administration.

Declaration of Competing Interest

The authors declare that they have no known competing financial interests or personal relationships that could have appeared to influence the work reported in this paper.

Data availability

Data will be made available on request.

Acknowledgements

This work has been carried out within the framework of the EUROfusion Consortium, funded by the European Union via the Euratom Research and Training Programme (Grant Agreement No 101052200 - EUROfusion). Views and opinions expressed are however those of the author(s) only and do not necessarily reflect those of the European Union or the European Commission. Neither the European Union nor the European Commission can be held responsible for them. The activity has been performed under EUROfusion work-package plasma facing components (WP-PFC, FP8).

References

[1] T. Hirai, et al., ITER tungsten divertor design development and qualification program, Fusion Eng. Des. 88 (9–10) (Oct. 2013) 1798–1801, https://doi.org/10.1016/j.fusengdes.2013.05.010.
[2] S. Brezinsek, et al., Plasma–wall interaction studies within the EUROfusion consortium: progress on plasma-facing components development and qualification, Nucl. Fusion 57 (11) (Nov. 2017), 116041, https://doi.org/10.1088/1741-4326/aa796e.
[3] M. Rasinski, et al., High resolution scanning transmission electron microscopy (HR STEM) analysis of re-deposited layer on ASDEX Upgrade tile, Fusion Eng. Des. 86 (9–11) (2011) 1753–1756, https://doi.org/10.1016/j.fusengdes.2011.02.085.
[4] E. Fortuna-Zalesna, et al., Post mortem analysis of a tungsten coated tile from the outer divertor strike point region of ASDEX upgrade, Nucl. Mater. Energy 9 (2016) 128–131, https://doi.org/10.1016/j.nme.2016.10.011.
[5] M. Mayer, et al., Tungsten erosion and redeposition in the all-tungsten divertor of ASDEX Upgrade, Phys. Scr. T138 (Dec. 2009), 014039, https://doi.org/10.1088/0031-8949/2009/T138/014039.
[6] M. Mayer, et al., Erosion and deposition in the JET divertor during the first ILW campaign, Phys. Scr. T167 (Feb. 2016), 014051, https://doi.org/10.1088/0031-8949/T167/1/014051.
[7] E. Fortuna-Zaleśna, et al., Studies of dust from JET with the ITER-Like Wall: Composition and internal structure, Nucl. Mater. Energy 12 (2017) 582–587, https://doi.org/10.1016/j.nme.2016.11.027.
[8] M. Balden, et al., Erosion and redeposition patterns on entire erosion marker tiles after exposure in the first operation phase of WEST, Phys. Scr. 96 (12) (Dec. 2021), 124020, https://doi.org/10.1088/1402-4896/ac2182.
[9] C. Martin, et al., First post-mortem analysis of deposits collected on ITER-like components in WEST after the C3 and C4 campaigns, Phys. Scr. 96 (12) (Dec. 2021), 124035, https://doi.org/10.1088/1402-4896/ac267e.
[10] S. Kajita, W. Sakaguchi, N. Ohno, N. Yoshida, T. Saeki, Formation process of tungsten nanostructure by the exposure to helium plasma under fusion relevant plasma conditions, Nucl. Fusion 49 (9) (Sep. 2009), 095005, https://doi.org/10.1088/0029-5515/49/9/095005.
[11] S. Möller, O. Kachko, M. Rasinski, A. Kreter, C. Linsmeier, In situ investigation of helium fuzz growth on tungsten in relation to ion flux, fluence, surface temperature and ion energy using infrared imaging in PSI-2, Phys. Scr. T170 (Dec. 2017), 014017, https://doi.org/10.1088/1402-4896/aa8a0a.
[12] R. Sakamoto, E. Bernard, A. Kreter, N. Yoshida, Surface morphology of tungsten exposed to helium plasma at temperatures below fuzz formation threshold 1073 K, Nucl. Fusion 57 (1) (2017) pp, https://doi.org/10.1088/1741-4326/57/1/016040.
[13] H.Y. Xu, et al., Observations of orientation dependence of surface morphology in tungsten implanted by low energy and high flux D plasma, J. Nucl. Mater. 443 (1–3) (2013) 452–457, https://doi.org/10.1016/j.jnucmat.2013.07.062.
[14] H.Y. Xu, et al., Enhanced modification of tungsten surface by nanostructure formation during high flux deuterium plasma exposure, J. Nucl. Mater. 447 (1–3) (2014) 22–27, https://doi.org/10.1016/j.jnucmat.2013.12.010.
[15] H.Y. Xu, et al., Deuterium-induced nanostructure formation on tungsten exposed to high-flux plasma, J. Nucl. Mater. 463 (2015) 308–311, https://doi.org/10.1016/j.jnucmat.2014.11.039.
[16] Y.Z. Jia, et al., Nanostructures and pinholes on W surfaces exposed to high flux D plasma at high temperatures, J. Nucl. Mater. 463 (2015) 312–315, https://doi.org/10.1016/j.jnucmat.2014.11.054.
[17] Y.Z. Jia, W. Liu, B. Xu, S.L. Qu, L.Q. Shi, T.W. Morgan, Subsurface deuterium bubble formation in W due to low-energy high flux deuterium plasma exposure, Nucl. Fusion 57 (3) (2017) pp, https://doi.org/10.1088/1741-4326/57/3/034003.
[18] Y.Z. Jia, W. Liu, B. Xu, S. L. Qu, T.W. Morgan, Surface nano structures on W surface exposed to low-energy high flux D plasma, Nucl. Instrum. Methods Phys. Res. Sect. B Beam Interact. Mater. At., vol. 438, no. August 2018, pp. 26–30, 2019, doi: 10.1016/j.nimb.2018.10.022.
[19] M. Sala, A. Uccello, D. Dellasega, M. Pedroni, E. Vassallo, M. Passoni, Exposures of bulk W and nanostructured W coatings to medium flux D plasmas, Nucl. Mater. Energy vol. 24, no. March (2020), 100779, https://doi.org/10.1016/j.nme.2020.100779.
[20] M. H. J. 't Hoen, D. Dellasega, A. Pezzoli, M. Passoni, A. W. Kleyn, P. A. Zeijlmans van Emmichoven, Deuterium retention and surface modifications of nanocrystalline tungsten films exposed to high-flux plasma, J. Nucl. Mater., vol. 463, pp. 989–992, Aug. 2015, doi: 10.1016/j.jnucmat.2014.11.025.
[21] D. Dellasega, G. Merlo, C. Conti, C.E. Bottani, M. Passoni, Nanostructured and amorphous-like tungsten films grown by pulsed laser deposition, J. Appl. Phys. 112 (8) (2012), 084328, https://doi.org/10.1063/1.4761842.
[22] A. Pezzoli, D. Dellasega, V. Russo, A. Gallo, P.A. Zeijlmans van Emmichoven, M. Passoni, Thermal annealing and exposure to divertor-like deuterium plasma of tailored tungsten oxide coatings, J. Nucl. Mater. 463 (Aug. 2015) 1041–1044, https://doi.org/10.1016/j.jnucmat.2014.11.035.
[23] A. Maffini, et al., In situ cleaning of diagnostic first mirrors: An experimental comparison between plasma and laser cleaning in ITER-relevant conditions, Nucl. Fusion 57 (4) (2017) pp, https://doi.org/10.1088/1741-4326/aa5d05.
[24] R. Mateus, et al., Helium load on W-O coatings grown by pulsed laser deposition, Surf. Coat. Technol. (2018), https://doi.org/10.1016/j.surfcoat.2018.02.089.
[25] E. Besozzi, D. Dellasega, A. Pezzoli, C. Conti, M. Passoni, M.G. Beghi, Amorphous, ultra-nano- and nano-crystalline tungsten-based coatings grown by Pulsed Laser Deposition: Mechanical characterization by Surface Brillouin Spectroscopy, Mater. Des. 106 (2016), https://doi.org/10.1016/j.matdes.2016.04.096.
[26] E. Besozzi, et al., Nanosecond laser pulses for mimicking thermal effects on nanostructured tungsten-based materials, Nucl. Fusion 58 (3) (2018) pp, https://doi.org/10.1088/1741-4326/aaa5d5.
[27] N. Ezumi, Zh. Kiss'ovski, W. Bohmeyer, G. Fussmann, Ion sensitive probe measurement in the linear plasma device PSI-2, J. Nucl. Mater. 337–339 (Mar. 2005) 1106–1110, https://doi.org/10.1016/j.jnucmat.2004.10.155.
[28] M. Mayer, SIMNRA, a simulation program for the analysis of NRA, RBS and ERDA, in: AIP Conference Proceedings, AIP, 1999, pp. 541–544. doi: 10.1063/1.59188.
[29] V. Nemanič, B. Zajec, D. Dellasega, M. Passoni, Hydrogen permeation through disordered nanostructured tungsten films, J. Nucl. Mater. 429 (1–3) (Oct. 2012) 92–98, https://doi.org/10.1016/j.jnucmat.2012.05.031.
[30] J.A. Thornton, The microstructure of sputter-deposited coatings, J. Vac. Sci. Technol. Vac. Surf. Films 4 (6) (Nov. 1986) 3059–3065, https://doi.org/10.1116/1.573628.
[31] D. Dellasega, et al., Tungsten oxide nanowires grown on amorphous-like tungsten films, Nanotechnology 26 (36) (Sep. 2015), 365601, https://doi.org/10.1088/0957-4484/26/36/365601.
[32] M. Balden, A. Manhard, S. Elgeti, Deuterium retention and morphological modifications of the surface in five grades of tungsten after deuterium plasma exposure, J. Nucl. Mater. 452 (1–3) (2014) 248–256, https://doi.org/10.1016/j.jnucmat.2014.05.018.
[33] M. H. J. 't Hoen,, et al., Surface morphology and deuterium retention of tungsten after low- and high-flux deuterium plasma exposure, Nucl. Fusion 54 (8) (2014) pp, https://doi.org/10.1088/0029-5515/54/8/083014.
[34] O.V. Ogorodnikova, K. Sugiyama, T. Schwarz-Selinger, T. Dürbeck, M. Balden, Ion-induced deuterium retention in tungsten coatings on carbon substrate, J. Nucl. Mater. 419 (1–3) (Dec. 2011) 194–200, https://doi.org/10.1016/j.jnucmat.2011.07.023.
[35] S. Möller, et al., Dynamic outgassing of deuterium, helium and nitrogen from plasma-facing materials under DEMO relevant conditions, Nucl. Fusion 57 (1) (2017) pp, https://doi.org/10.1088/0029-5515/57/1/016020.
[36] H.Y. Xu, et al., Blistering on tungsten surface exposed to high flux deuterium plasma, J. Nucl. Mater. 471 (2016) 51–58, https://doi.org/10.1016/j.jnucmat.2015.12.025.
[37] S.B. Singh, N. Chand, D.S. Patil, Langmuir probe diagnostics of microwave electron cyclotron resonance (ECR) plasma, Vacuum 83 (2) (Sep. 2008) 372–377, https://doi.org/10.1016/j.vacuum.2008.05.030.
[38] T.K. Popov, et al., Advances in Langmuir probe diagnostics of the plasma potential and electron-energy distribution function in magnetized plasma, Plasma Sources Sci. Technol. 25 (3) (Jun. 2016), 033001, https://doi.org/10.1088/0963-0252/25/3/033001.

[39] W. Guo, et al., Nanostructure evolution and surface modification of tungsten exposed to low energy, high flux deuterium plasma, Fusion Eng. Des. 125 (2017) 473–478, https://doi.org/10.1016/j.fusengdes.2017.04.057.
[40] A. Dunand, M. Minissale, J.-B. Faure, L. Gallais, T. Angot, R. Bisson, Surface oxygen versus native oxide on tungsten: contrasting effects on deuterium retention and release, Nucl. Fusion 62 (5) (May 2022), 054002, https://doi.org/10.1088/1741-4326/ac583a.
[41] Z. Tian, J.W. Davis, A.A. Haasz, Deuterium retention in tungsten at fluences of up to 1026 D+/m2 using D+ ion beams, J. Nucl. Mater. 399 (1) (Apr. 2010) 101–107, https://doi.org/10.1016/j.jnucmat.2010.01.007.
[42] M. Reinhart, et al., Influence of plasma impurities on the deuterium retention in tungsten exposed in the linear plasma generator PSI-2, J. Nucl. Mater. 463 (Aug. 2015) 1021–1024, https://doi.org/10.1016/j.jnucmat.2014.11.045.
[43] H. Zhang, X. Zhang, L. Qiao, P. Wang, Deuterium retention in tungsten and tungsten alloys exposed to pure and impurities seeding deuterium plasma, Nucl. Mater. Energy 25 (Dec. 2020), 100822, https://doi.org/10.1016/j.nme.2020.100822.
[44] T. Sakai et al., Effect of Deuterium Fluence on Deuterium Retention in Tungsten with Fibrous Nanostructured Layer in a Compact Plasma Device APSEDAS, Plasma Fusion Res., vol. 17, no. 0, pp. 2405062–2405062, Jun. 2022, doi: 10.1585/pfr.17.2405062.
[45] O.V. Ogorodnikova, et al., Deuterium retention in dense and disordered nanostructured tungsten coatings, J. Nucl. Mater. 507 (2018), https://doi.org/10.1016/j.jnucmat.2018.04.039.
[46] A. Uccello, et al., Effects of a nitrogen seeded plasma on nanostructured tungsten films having fusion-relevant features, Nucl. Mater. Energy 25 (2020), https://doi.org/10.1016/j.nme.2020.100808.
[47] P. Paris, et al., In-situ LIBS and NRA deuterium retention study in porous W-O and compact W coatings loaded by Magnum-PSI, Fusion Eng. Des. 168 (2021), https://doi.org/10.1016/j.fusengdes.2021.112403.
[48] I. Jõgi, et al., LIBS study of ITER relevant tungsten–oxygen coatings exposed to deuterium plasma in Magnum-PSI, J. Nucl. Mater. 544 (2021), 152660, https://doi.org/10.1016/j.jnucmat.2020.152660.